J. Fluid Mech. (1991), *vol.* 231, *pp.* 303–324
Printed in Great Britain

Coastal Kelvin waves in the presence of a slowly varying topography

By PING CHANG†
The Joint Institute of the Study of the Atmosphere and Oceans, University of Washington, AK-40, Seattle, WA 98195, USA

(Received 27 August 1990 and in revised form 14 March 1991)

The evolution equation is derived for a weakly nonlinear coastal Kelvin wave propagating in slowly varying topography in an f-plane ocean. For weak transverse variations in the topography, the wave evolution is governed by a perturbed Korteweg–de Vries equation. In the absence of transverse variation, wave dispersion vanishes and the evolution equation reduces to a nonlinear advection equation with variable coefficients. As a general property of these equations, the total mass flux associated with the Kelvin wave is not conserved; residual mass must be generated. It is shown by an asymptotic analysis that this residual mass field is in balance with a mean geostrophic current long after the passage of the Kelvin wave. This result is verified using a numerical model. The physical mechanism evolved in the generation of the residual mass can be understood in terms of potential vorticity conservation.

1. Introduction

Kelvin waves are known to play an important role in the oceanic adjustment near boundaries and the equator (Gill 1982). The classical Kelvin wave is a trapped wave solution in a rotating, semi-infinite, shallow-water ocean of uniform depth H bounded by a vertical wall. It is a linear, non-dispersive wave propagating along the boundary with the phase speed $C = (gH)^{\frac{1}{2}}$ in the direction of rotation. Since such a classical solution neglects the effects due to nonlinearity and varying mean backgrounds (such as topography and mean currents), it has little application to real oceans.

During the past two decades, studies of Kelvin waves have attempted to include these effects. Smith (1972) and Grimshaw (1977) demonstrated that offshore topography can introduce a topographic dispersion to Kelvin waves. For a weakly nonlinear wave, this dispersion may balance the nonlinearity so that the evolution of the Kelvin wave is governed by the Korteweg–de Vries (KdV) equation. On the other hand, Miles (1972, 1973) considered the effects of variation in alongshore topography, Earth's curvature and coastline geometry. He showed that alongshore-varying topography can cause substantial changes in the amplitude and phase speed of Kelvin waves. If the topography varies slowly along the coastline, wave energy is approximately conserved. The Kelvin wave evolves according to Green's law; that is the vertical displacement of the free surface associated with the Kelvin wave is inversely proportional to the square root of the depth of the fluid. However, if the topography varies abruptly as a step function, a Kelvin wave can be diffracted at the step. Miles (1973) showed that the wave diffraction can be calculated by solving a

† Present address: Department of Oceanography, Texas A&M University, College Station, TX 77843, USA.

singular integral equation whose solution is intractable without further approximation. More recently, Killworth (1989*a*, *b*) generalized the problem by considering the interaction between a Kelvin wave and a smooth ridge of width comparable to the deformation radius extending uniformly away from the coastline. Although no analytical solutions were found, it was shown that simple bounds may be placed on the amplitude of the transmitted Kelvin wave using calculus of variations method.

Studies of water waves propagating in a channel of variable depth in a non-rotating system can be dated back to Boussinesq who in 1872 recognized that, when a long surface wave propagates in a channel of gradually varying depth, a slow change in wave amplitude must occur to satisfy the principle of conservation of energy. However, he also realized that, even allowing for this wave amplitude modulation, the mass flux associated with the wave was not conserved. This seeming paradox has been the subject of many investigations (Johnson 1973; Grimshaw 1983; Miles 1979; Knickerbocker & Newell 1980, 1985). It is now understood that the non-conservation of mass flux is caused by wave reflection which is neglected in the wave evolution equation – the perturbed Korteweg–de Vries (PKdV) equation. Studies by Miles (1979) and Knickerbocker & Newell (1985) have demonstrated that the total mass flux is resolved into a primary (KdV) flux and a residual flux that is proportional to the mean displacement of the primary wave. The reflected waves are small-amplitude (relative to the primary wave), non-dispersive, long waves which travel in the direction opposite to the primary wave and stretch over a distance much longer than the primary wavelength. These waves, in turn, carry a mass flux of equal order to the primary mass flux.

Recently, Long & Chang (1990) have applied these concepts to a rotating ocean. The problem they considered was an equatorially trapped Kelvin wave propagating in a slowly varying thermocline which was assumed to be balanced by the wind forcing. Using a multiple scale analysis, it was shown that the evolution of wave amplitude riding with the equatorial Kelvin wave was governed by a PKdV equation. This equation, just like the PKdV equation derived in a non-rotating fluid, cannot conserve mass. Thus, the residual mass is generated in the wake of the Kelvin wave. Although they did not analytically solve for the residual mass flux, numerical simulations indicated that the residual mass was carried westward by the long, non-dispersive Rossby waves. In the present study, we consider the problem of a coastal Kelvin wave propagating in a rotating fluid with depth variations in both the offshore and alongshore directions. The topography here is assumed to be a linear superposition of a slowly varying alongshore oscillation and a small-amplitude offshore topography. The fundamental difference between this problem and the previous one is that the long, non-dispersive Rossby waves which existed in the equatorial β-plane are absent here to the lowest order. Since these waves are crucial in transporting the residual mass, one may wonder what happens to the mass flux associated with an f-plane Kelvin wave as it propagates in a slowly varying topography. In particular, does an f-plane Kelvin wave pulse conserve its mass flux? If not, how is the residual mass adjusted on an f-plane ocean?

In §2 we show that the nonlinear evolution of a Kelvin wave in the presence of a slowly varying two-dimensional topography is governed by a PKdV equation similar to the one derived by Long & Chang (1990). Thus, the primary mass flux associated with the Kelvin wave is not conserved. We then show in §3 that the residual mass flux is generated from the interaction between the Kelvin wave and the topography. By explicitly solving the high-order perturbation equations, we further show that the asymptotic solutions represent a wave-adjustment process similar to the classical

geostrophic adjustment. In §4 the numerical simulations of the full shallow-water equations are given in support of the analytical solutions. Finally, in §5 we discuss the results from the point of view of potential vorticity conservation.

2. Derivation of the perturbed KdV equation

The perturbed KdV equation was first derived by Johnson (1973) and Kakutani (1971) to describe the appropriate nonlinear evolution of a long surface wave propagating in a non-rotating channel of variable depth. We show in this section that the time evolution of a weakly nonlinear f-plane Kelvin wave in the presence of a slowly varying two-dimensional topography is described by a similar type of equation. The perturbation techniques used here are essentially the same as those described by Long & Chang (1990) in the study of an equatorial Kelvin wave in the presence of a varying thermocline. Therefore, in the interests of brevity we shall omit the detailed analyses and quote merely the important solutions.

Consider a semi-infinite inviscid reduced-gravity shallow-water ocean, rotating with angular velocity $\frac{1}{2}f$ about a vertical axis, bounded by a wall in the west. The equations of motion are given by

$$\partial_t u+\epsilon(u\,\partial_x u+v\,\partial_y u)-fv=-g'\,\partial_x h; \tag{1}$$

$$\partial_t v+\epsilon(u\,\partial_x v+v\,\partial_y v)+fu=-g'\,\partial_y h; \tag{2}$$

$$\partial_t h+\bar{h}(\partial_x u+\partial_y v)+u\,\partial_x \bar{h}+v\,\partial_y \bar{h}+\epsilon[\partial_x(hu)+\partial_y(hv)]=0, \tag{3}$$

where the small parameter ϵ measures the amplitude of the perturbation field, $\bar{h}$ is the layer thickness at rest, which includes the variation of topography; f is the Coriolis parameter and is a constant under the f-plane assumption, g' is the reduced gravity and h is the perturbation of the layer thickness. A no-flux boundary condition at the western boundary implies that u must vanish at $x=0$.

To allow the nonlinearity and wave dispersion to enter at the same order, we assume that the topography $\bar{h}$ has the form

$$\bar{h}=H(y)+\epsilon^{\frac{1}{2}}\Psi(x). \tag{4}$$

Substitution of (4) into (3) gives

$$\partial_t h+(C^2/g+\epsilon^{\frac{1}{2}}\Psi)\,\partial_x u+\partial_y v)+\epsilon^{\frac{1}{2}}\Psi_x u+2/g\,CC_y v+\epsilon[\partial_x(hu)+\partial_y(hv)]=0, \tag{5}$$

where $C=(g'H(y))^{\frac{1}{2}}$ is the local shallow-water wave speed in the absence of offshore topography. Assuming that the alongshore lengthscale of the topography is much greater than the scale of the waves, we can introduce a slow variable and a fast variable:

fast-time variable† $s=(1+\epsilon^{\frac{1}{2}}\omega_1+\epsilon\omega_2+\ldots)\,t$;
fast-space variable $\eta=y$;
slow-space variable $Y=\epsilon y$,

where ω_i, $(i=1,2,\ldots)$ is a set of parameters which needs to be determined. Since C is a function of the slow variable Y, we can introduce the following phase coordinates:

$$\sigma=s+\int^{\eta}\frac{\mathrm{d}\eta'}{C(\epsilon\eta')}\quad\text{and}\quad\tau=s-\int^{\eta}\frac{\mathrm{d}\eta'}{C(\epsilon\eta')}. \tag{6}$$

† Alternatively, we can choose $s=t$ as a fast-time variable, and then replace C^{-1} in the phase coordinates, (6), by $C_s^{-1}=C^{-1}(1+\epsilon^{\frac{1}{2}}\omega_1+\epsilon\omega_2+\ldots)$. This choice of the variables eventually leads to the same solutions.

Substituting these new coordinates into (1), (2) and (3), and expanding u, v and h in power series of $\epsilon^{\frac{1}{2}}$, we find a Kelvin wave solution at $O(\epsilon^0)$:

$$u_0 = 0; \tag{7}$$

$$v_0 = A(\sigma; Y)\exp(-f/Cx); \tag{8}$$

$$h_0 = -C/g' A(\sigma; Y)\exp(-f/Cx), \tag{9}$$

where $A(\sigma; Y)$ is an arbitrary function at this order. Note that solutions depend on σ only, indicating that the Kelvin wave always propagates towards the equator along the western boundary.

At next order ($O(\epsilon^{\frac{1}{2}})$), the forcing terms on the right-hand side of the perturbation equations do not contain nonlinear terms. The non-secularity condition is applied merely to determine the phase-speed correction ω_1 at this order:

$$\omega_1 = fg'/C^3 \int_0^\infty \Psi \exp(-2f/Cx)\,\mathrm{d}x. \tag{10}$$

Proceeding to $O(\epsilon)$, the governing perturbation equations at $O(\epsilon)$ contain both dispersion and nonlinearity. To identify the secularities at this order, it is necessary to solve for the particular solutions at $O(\epsilon^{\frac{1}{2}})$ which are independent of τ. This can be achieved by expanding the $O(\epsilon^{\frac{1}{2}})$ solutions in terms of a set of complete eigenmodes in a semi-infinite f-plane which consists of a continuum of Poincaré modes and a coastal Kelvin mode. Collecting all the secularities (terms that are independent of τ) in the second-order forcing, the non-secularity condition then gives the perturbed KdV equation for wave amplitude A in the form

$$2CC_Y A + C^2 \partial_Y A - A\,\partial_\sigma A + M\,\partial_\sigma^3 A = 0, \tag{11}$$

and the phase-speed correction in the form

$$\omega_2 = -\omega_1^2 + \frac{2g'^2 f}{\pi C^7}\int_0^\infty \frac{1}{(k^2 + f^2/C^2)}\left[\int_0^\infty \Psi \sin kx \exp\left(-\frac{f}{C}x\right)\mathrm{d}x\right]^2 \mathrm{d}k, \tag{12}$$

where M measures the strength of dispersion caused by offshore topography Ψ and is given by

$$M = \frac{2g'^2 f^3}{\pi C^8}\int_0^\infty \frac{1}{(k^2 + f^2/C^2)^2}\left[\int_0^\infty \Psi\left(\sin kx - \frac{C}{f}k\cos kx\right)\exp\left(-\frac{f}{C}x\right)\mathrm{d}x\right]^2 \mathrm{d}k. \tag{13}$$

As a check on the asymptotic solution, consider a special case in which $\Psi = \Psi_0 =$ constant, then

$$M = 0; \quad \omega_1 = \frac{g'\Psi_0}{2C^2}; \quad \omega_2 = -\frac{g'^2\Psi_0^2}{8C^4}.$$

This result is consistent with the expansion of the total shallow-water wave speed in the absence of offshore topography, i.e.

$$C_s = (C^2 + \epsilon^{\frac{1}{2}} g'\Psi_0)^{\frac{1}{2}} = C\left(1 + \frac{g'\Psi_0}{2C^2}\epsilon^{\frac{1}{2}} - \frac{g'^2\Psi_0^2}{8C^4}\epsilon + \ldots\right).$$

In deriving the perturbed KdV equation, the WKB assumption that the scale of the Kelvin wave pulse is much smaller than the scale of the topography implies that

the Kelvin wave described by (11) will undergo an adiabatic change in amplitude to (approximately) conserve energy. If we substitute (7), (8) and (9) into the energy equation, it is readily shown that the energy density for a Kelvin wave to $O(\epsilon)$ is proportional to

$$E = \int_0^\infty v_0^2 H \, \mathrm{d}x = \frac{c}{2f} H A^2$$

and the energy flux is equal to

$$F = \int_0^\infty g' v_0 h_0 H \, \mathrm{d}x = CE.$$

On the other hand, multiplying (11) by A and then integrating with respect to σ from σ_0 to ∞ yields

$$\frac{\partial}{\partial Y} \int_{\sigma_0}^\infty C^4 A^2 \, \mathrm{d}\sigma = 0. \tag{14}$$

This means that the energy flux associated with a Kelvin wave pulse is indeed conserved to $O(\epsilon)$. In the linear regime, conservation of wave energy (equation (14)) implies that the longshore velocity component and height field of the Kelvin wave varies as the layer depth $H(Y)$ to the power of -1 and $-\frac{1}{2}$, respectively. This result is consistent with Miles' (1973) finding. In comparison with the classical Green's law found for shallow-water waves impinging on a beach (see, for example, Newell 1985), the power appearing in the analogue of the Green's law is increased by a factor of two.

Apart from the energy constraint, a wave pulse is also subject to its mass constraint. It is widely known that the perturbed KdV equation (11) does not satisfy the mass conservation law to the same order as energy conservation (see, for example, Newell 1985; Grimshaw 1983). To illustrate this point, we consider a simple case in which wave dispersion is absent. The solution to (11), in the linear regime, is governed by Green's law, i.e.

$$A = G(\sigma) H^{-1}(Y). \tag{15}$$

The mass transport associated with a Kelvin wave pulse is then given by

$$M_{\mathrm{Kel}} = \int_0^\infty \int_0^\infty \mathrm{d}t \, \mathrm{d}x (H v_0) = \left(\frac{1}{f} \int_{\sigma_0}^\infty G \, \mathrm{d}\sigma \right) C(Y). \tag{16}$$

Equation (16) shows that the mass transport associated with a Kelvin wave varies along topography, indicating that the mass is not conserved.

The non-conservation of mass implies that a certain portion of the mass associated with the Kelvin wave pulse must be left behind. A detailed analysis of what happens in the wake of a Kelvin wave pulse will be given in the next section. Here, without solving for the detailed solutions, we estimate how much residual mass is generated by the topography. Imagine a small-amplitude Kelvin wave pulse propagating through monotonically varying topography from a initially uniform layer depth H_1 to a new constant depth H_2, as shown in figure 1. Since no interaction between the topography and Kelvin wave can occur after the wave has reached H_2, residual mass cannot be generated beyond that point. On the other hand, the total mass flux is equal to the sum of the residual mass flux and the mass flux associated with the

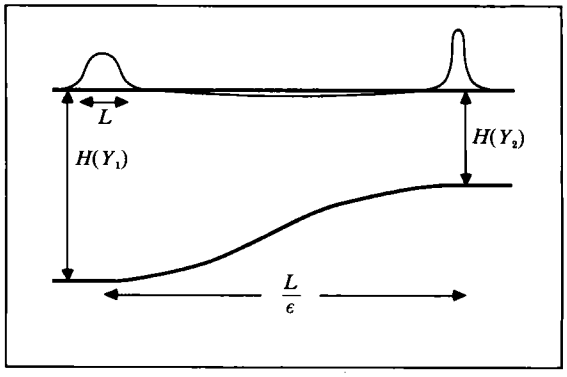

FIGURE 1. A sketch of the physical system being considered. A Kelvin wave pulse propagates through a montonically varying topography from an initial uniform layer depth $H_1 = H(Y_1)$ to a new constant depth $H_2 = H(Y_2)$. The scale of the wave is $O(L)$, whereas the scale of the topography is $O(L/\epsilon)$.

Kelvin wave. By mass conservation, the total mass flux must be equal to the mass flux associated with the Kelvin wave pulse after it has reached the new constant depth H_2. Consequently, the residual mass flux at any given location Y is equal to the difference between the mass flux associated with the Kelvin wave at $H(Y)$ and H_2, namely,

$$M_{\text{Res}} = \frac{1}{f}\int_{\sigma_0}^{\infty} G\,\mathrm{d}\sigma[(g'H(Y))^{\frac{1}{2}} - (g'H_2)^{\frac{1}{2}}]. \tag{17}$$

Therefore, the total amount of residual mass over the topography (between H_1 and H_2) can be obtained by letting $H(y) = H_1$ in (17). Evidently, this residual mass flux is comparable in magnitude with the primary mass flux. The apparent inconsistency between the conservation of mass and of energy associated with a Kelvin wave pulse can be explained qualitatively using scaling arguments as shown in Newell (1985) and Long & Chang (1990).

3. Adjustment of residual mass

The solutions obtained in the previous section indicate that a substantial portion of mass associated with the Kelvin wave is lost as it passes through a slowly varying topography. In this section we explicitly solve for $O(\epsilon)$ perturbation solutions in order to understand how this residual mass is adjusted on an f-plane.

For simplicity, we neglect the offshore variation in the topography, because it does not fundamentally change the characteristic of the problem. To do that, we set $\Psi = 0$ in (5) and expand the solution in a power series in ϵ. The lowest-order solutions are still given by (7), (8) and (9) and the first-order ($O(\epsilon)$) perturbation equations read

$$\partial_t u - fv + g'\,\partial_x h = 0; \tag{18}$$

$$\partial_t v + fu + g'\,\partial_\eta h = -(g'\,\partial_Y h_0 + v_0\,\partial_\eta v_0); \tag{19}$$

$$\partial_t h + [C^2(Y)/g'](\partial_x u + \partial_\eta v) = -[(1/g')\,\partial_Y(C^2 v_0) + \partial_\eta(h_0 v_0)]. \tag{20}$$

To obtain solutions to the above equations, we use the method described by Gill (1982). First, we combine (18), (19) and (20) to derive two equations governing the

offshore velocity component of u and the layer-averaged perturbed potential vorticity q,

$$\partial^2 u/\partial t^2 + f^2 u - C^2 \nabla^2 u - g' \partial q/\partial \eta = 3 f v_0 \partial v_0/\partial \eta \tag{21}$$

and

$$\partial q/\partial t = f/g' \, \partial C^2/\partial Y \, v_0, \tag{22}$$

where $q = \partial_x(Hv) - \partial_\eta(Hu) - fh$, which is an invariant of the system in the absence of topography. Equation (22) indicates that q is generated from the interaction between the primary Kelvin wave and topography. Eliminating q from (21) and (22), using the initial condition $u = v = h = q = 0$, at $t = 0$, we have

$$\frac{\partial^2 u}{\partial t^2} + f^2 u - C^2 \nabla^2 u = f \frac{\partial C^2}{\partial Y} \int_0^t \frac{\partial v_0}{\partial \eta} \mathrm{d}t + 3 f v_0 \frac{\partial v_0}{\partial \eta}. \tag{23}$$

In contrast to the classical Rossby adjustment problem considered by Gill (1976, 1982), the offshore velocity component is not forced by the initial potential vorticity perturbation, but rather by the potential vorticity anomalies induced by Kelvin wave–topography interaction and by the nonlinear self-interaction of the Kelvin wave. At this stage, it is convenient to introduce the phase coordinates defined in (6) and (23):

$$4 \frac{\partial^2 u}{\partial \sigma \, \partial \tau} + f^2 u - C^2 \frac{\partial^2 u}{\partial x^2} = 2 f \frac{\partial C}{\partial Y} v_0 + 3 f v_0 \frac{\partial v_0}{\partial \eta}. \tag{24}$$

Here, without losing generality, we have assumed that the Kelvin wave pulse starts at a position where the fluid depth is uniform, so that the interaction between the Kelvin wave and topography is zero at $t = 0$. The proper boundary conditions to (24) are that u has to vanish at $x = 0$ and to be bounded as $x \to \infty$.

The solution to (24), in general, consists of two parts: a homogeneous part u^{h} and a forced part u^{f}. The homogeneous part of the solution represents Poincaré waves. Since we are not interested in the details of Poincaré waves, the homogeneous solutions to (23) can be simply written as $u^{\mathrm{h}} = u^{\mathrm{h}}(\sigma, \tau; Y, x)$. However, it is important to point out that to avoid a trivial solution, u^{h} must be a function of both σ and τ.

The forced part of the solution, subject to the boundary condition $u = 0$, at $x = 0$, is given by

$$u^{\mathrm{f}} = \frac{1}{C} \frac{\partial C}{\partial Y} A x \exp\left(-\frac{f}{C} x\right) + \frac{1}{Cf} A \frac{\partial A}{\partial \sigma} \left[\exp\left(-\frac{f}{C} x\right) - \exp\left(-\frac{2f}{C} x\right)\right]. \tag{25}$$

Note that u^{f} tends to follow the motion of the primary Kelvin wave, and thus it cannot leave a permanent signature behind the Kelvin wave.

Once u has been determined, we find it convenient to obtain v and h by defining two Riemann invariants

$$S = v - g'/C \, h \quad \text{and} \quad R = v + g'/C \, h, \tag{26}$$

where S and R satisfy the following equations:

$$2 \frac{\partial S}{\partial \tau} = -f u^{\mathrm{h}} + C \frac{\partial u^{\mathrm{h}}}{\partial x} + \frac{2}{C} \left[\frac{\partial}{\partial Y}(C^2 A) - A \frac{\partial A}{\partial \sigma}\right] \exp\left(-\frac{f}{C} x\right); \tag{27}$$

$$2 \frac{\partial R}{\partial \sigma} = -f u^{\mathrm{h}} - C \frac{\partial u^{\mathrm{h}}}{\partial x} - 2 \frac{\partial C}{\partial Y} A \exp\left(-\frac{f}{C} x\right). \tag{28}$$

Since the last term on the right-hand side of (27) depends on σ only, it must vanish to ensure that the equation is non-secular. This condition gives us an evolution equation for the wave amplitude A in the form of

$$\frac{\partial}{\partial Y}(C^2A)-A\frac{\partial A}{\partial\sigma}=0, \tag{29}$$

which is precisely the PKdV equation (11) in the absence of wave dispersion. After eliminating the secularity in (27), solutions for v and h can be easily obtained, using (26), from (27) and (28):

$$v=v^{\mathrm{h}}-\frac{1}{2}\frac{\partial C}{\partial Y}\int_{\sigma_0}^{\sigma}A\,\mathrm{d}\sigma\exp\left(-\frac{f}{C}x\right)+\tfrac{1}{2}[\Theta(\tau;Y,x)+\Phi(\sigma;Y,x)]; \tag{30}$$

$$h=h^{\mathrm{h}}-\frac{C}{2g'}\frac{\partial C}{\partial Y}\int_{\sigma_0}^{\sigma}A\,\mathrm{d}\sigma\exp\left(-\frac{f}{C}x\right)+\frac{C}{2g'}[\Theta(\tau;Y,x)-\Phi(\sigma;Y,x)], \tag{31}$$

where Φ and Θ are arbitrary functions which need to be determined; v^{h} and h^{h} are the homogeneous part of the solution in v and h and are given by

$$v^{\mathrm{h}}=-\tfrac{1}{4}\{f[\overline{(u^{\mathrm{h}})}^{\sigma}+\overline{(u^{\mathrm{h}})}^{\tau}]+C\,\partial/\partial x\,[\overline{(u^{\mathrm{h}})}^{\sigma}-\overline{(u^{\mathrm{h}})}^{\tau}]\}, \tag{32}$$

$$h^{\mathrm{h}}=-C/4g'\{f[\overline{(u^{\mathrm{h}})}^{\sigma}-\overline{(u^{\mathrm{h}})}^{\tau}]+C\,\partial/\partial x\,[\overline{(u^{\mathrm{h}})}^{\sigma}+\overline{(u^{\mathrm{h}})}^{\tau}]\}, \tag{33}$$

respectively, where $\overline{(\ldots)}^{\tau}=\int_{\tau_0}^{\tau}(\ldots)\,\mathrm{d}\tau$ and $\overline{(\ldots)}^{\sigma}=\int_{\sigma_0}^{\sigma}(\ldots)\,\mathrm{d}\sigma$.

To determine Φ and Θ, we substitute (30) and (31) to (18) and then use the condition that v and h are bounded as $x\to\infty$. Finally, we obtain the perturbation solution v and h at $O(\epsilon)$:

$$\begin{aligned}v=&\left(\frac{f}{C}x-1\right)\frac{\partial C}{\partial Y}\int_{\sigma_0}^{\sigma}A\,\mathrm{d}\sigma\exp\left(-\frac{f}{C}x\right)\\&+\frac{2}{fC^2}\left[\left(\frac{\partial A}{\partial\sigma}\right)^2-A\frac{\partial^2A}{\partial\sigma^2}\right]\left[x+\frac{C}{f}\left(\exp\left(-\frac{f}{C}x\right)-1\right)\right]\exp\left(-\frac{f}{C}x\right)\\&+\frac{1}{2C^2}\frac{\partial C}{\partial Y}\frac{\partial A}{\partial\sigma}x^2\exp\left(-\frac{f}{C}x\right)+v^{\mathrm{h}},\end{aligned} \tag{34}$$

$$\begin{aligned}h=&-\frac{f}{g'}x\frac{\partial C}{\partial Y}\int_{\sigma_0}^{\sigma}A\,\mathrm{d}\sigma\exp\left(-\frac{f}{C}x\right)\\&-\frac{1}{fg'C}\left[\left(\frac{\partial A}{\partial\sigma}\right)^2-A\frac{\partial^2A}{\partial\sigma^2}\right]\left[x+\frac{C}{f}\left(\exp\left(-\frac{f}{C}x\right)-1\right)\right]\exp\left(-\frac{f}{C}x\right)\\&-\frac{1}{2g'C}\frac{\partial C}{\partial Y}\frac{\partial A}{\partial\sigma}x^2\exp\left(-\frac{f}{C}x\right)+h^{\mathrm{h}}.\end{aligned} \tag{35}$$

Here we have also used the condition that, at any given y, $\int_0^{\infty}v\,\mathrm{d}x$ must vanish after all the wave transients have propagated away. Solutions (34) and (35) consist of a geostrophically balanced current (the first terms on the right in (34) and (35)) and a transient wave solution which contains both a Kelvin wave and Poincaré wave. The physical process represented by these solutions is a geostrophic adjustment, i.e. gravity waves adjust the residual mass field to generate a geostrophic circulation. As

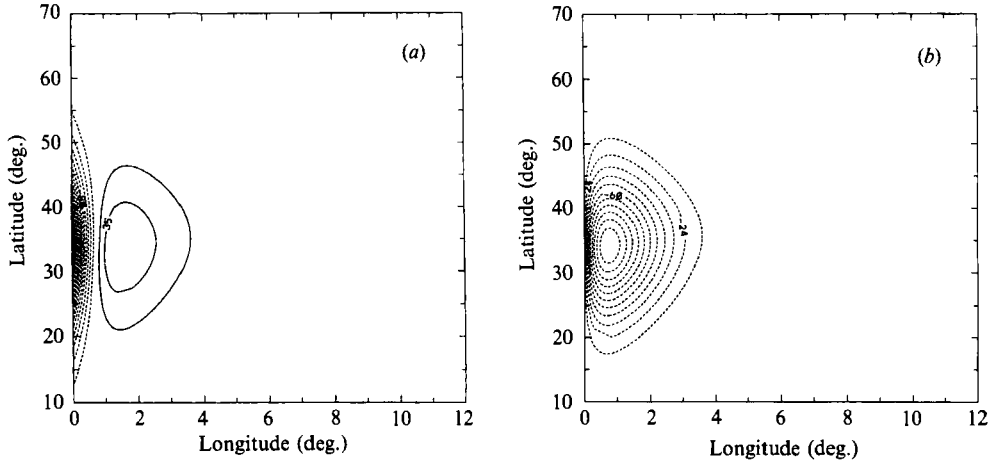

FIGURE 2. Contour plots of the asymptotic solutions described in the text for (*a*) the alongshore velocity component v and (*b*) the height field h, showing a geostrophic residual circulation situated over the topography.

a result, with increasing time, the wave transients will radiate away and the solution will approach a geostrophically balanced circulation:

$$v \to \left(\frac{f}{C}x - 1\right)\frac{\partial C}{\partial Y}\int_{\sigma_0}^{\sigma} A\,\mathrm{d}\sigma \exp\left(-\frac{f}{C}x\right) \quad \text{as} \quad \sigma \to \infty; \tag{36}$$

$$h \to -\frac{f}{g'}x\frac{\partial C}{\partial Y}\int_{\sigma_0}^{\sigma} A\,\mathrm{d}\sigma \exp\left(-\frac{f}{C}x\right) \quad \text{as} \quad \sigma \to \infty. \tag{37}$$

Figure 2 shows an example of the geostrophic residual circulation generated by a Kelvin wave pulse passing through a hyperbolic tangent topography, using parameters typical of the numerical solutions given in §4. Here v and h are calculated according to (36) and (37). The resulting circulation exhibits a relatively strong, narrow current against the boundary and a weak, broad returning flow in the interior. This picture is in good qualitative agreement with the numerical solution to be introduced in the next section.

Solutions (36) and (37) represent stationary circulation over the topography. Since these solutions show no sign of propagation in the offshore direction, it implies that topographic waves do not enter the solution at this order. This result is consistent with the assumption we made about the variation of the topography. Since the topography is assumed to be slowly varying, the topographic β-effect given by $\mathrm{d}(fH)\,\mathrm{d}y$ is on the order of ϵ. The change of potential vorticity induced by the wave disturbances $v\,\mathrm{d}(f/H)/\mathrm{d}y$ is then on the order of ϵ^2, which cannot balance the time rate of change of the wave potential vorticity (see (22)). Consequently, the topographic waves cannot occur at this order. However, the topographic waves will be important if the scale of topography becomes comparable to or smaller than the scale of the Kelvin wave. We shall verify this argument in terms of numerical experiments in the next section.

Finally, as a check on our solutions, again consider the case in which (15) is valid.

The total amount of residual mass can be calculated by integrating (37) over the topography, which gives

$$M_{\mathrm{Res}} = \epsilon \int_0^{\infty} \int_{y_1}^{y_2} h \, \mathrm{d}x \, \mathrm{d}y = \frac{1}{f}[(g'H_1)^{\frac{1}{2}} - (g'H_2)^{\frac{1}{2}}] \int_{\sigma_0}^{\sigma} G(\sigma) \, \mathrm{d}\sigma \quad \text{as} \quad \sigma \to \infty, \tag{38}$$

where $H_1 = H(Y_1)$ and $H_2 = H(Y_2)$ are the uniform layer depths shown in figure 1. This result is consistent with the estimation given in the previous section.

4. Numerical solutions

In this section we verify the analytical results obtained in the previous sections by numerically integrating the full shallow-water equations (1)–(3). Following Arakawa & Lamb (1981), we first rewrite the momentum equations (1) and (2) in a flux form in terms of potential vorticity $q = (f+\zeta)/(\bar{h}+h)$ and the energy density $E = \frac{1}{2}(u^2+v^2)+g'(\bar{h}+h)$. Then we discretize the governing equations on the staggered 'C' grid, using the second-order centred difference in space and the leap-frog scheme in time. The choice of the 'C' grid is based on the fact that it best simulates the geostrophic adjustment mechanism (Arakawa & Lamb 1977). The nonlinear terms in the equations are uniquely arranged so that the finite-difference analogues of (1), (2) and (3) satisfy conservation of energy and potential enstrophy constraints. It has been shown by Arakawa & Lamb (1981) that the potential enstrophy and energy conserving scheme has superiority over other schemes in dealing with flow over steep-topography problems. To remove the computational mode associated with the leap-frog scheme, a weak Robert smooth with a coefficient of 0.005 is used every time step. Otherwise, there is no explicit diffusion or dissipation in the model. The resolution of the model is 0.1° in both x and y. The model parameters are chosen to be the following: the mean depth of the reduced-gravity ocean H_0 has a value 1225 m and the reduced gravity g' has a value 4×10^{-2} m s^{-2}. This gives a shallow-water wave speed C_0 of 7 m s^{-1}. The model basin has a latitudinal width of 12° and a zonal length of 70°. The topography in the model is given by

$$\bar{h}(y) = H_0 \left\{ 1 + \frac{\delta}{2} \left[\tanh\left(\frac{y-y_c}{L_y} \right) - 1 \right] \right\}, \tag{39}$$

where δ is the amplitude of the alongshore variation in the layer depth, L_y is the alongshore lengthscale of the topography, y_c is the central location of the slope. For the initial conditions, we use the lowest-order asymptotic solution (7)–(9) with $A(x)$ being a Gaussian, namely

$$u(x, y, t = 0) = 0; \tag{40a}$$

$$v(x, y, t = 0) = \frac{C_0}{\Delta} \exp\left[-\left(\frac{y-y_0}{\Delta} \right)^2 - \left(\frac{x}{L_R} \right) \right]; \tag{40b}$$

$$h(x, y, t = 0) - \frac{H_0 C(y)}{\Delta C_0} \exp\left[-\left(\frac{y-y_0}{\Delta} \right)^2 - \left(\frac{x}{L_R} \right) \right], \tag{40c}$$

where Δ is an amplitude parameter, y_0 is the initial location of the Kelvin wave, Λ is the alongshore lengthscale of the wave and L_R is the local radius of deformation, i.e. $L_R = f/C$.

First, we present detailed results from one run with $\delta = 0.3$, $y_c = 35°$, $L_y = 10°$, and $\Delta = 500$, $y_0 = 64°$, $\Lambda = 2°$. This choice of the parameters approximately satisfies

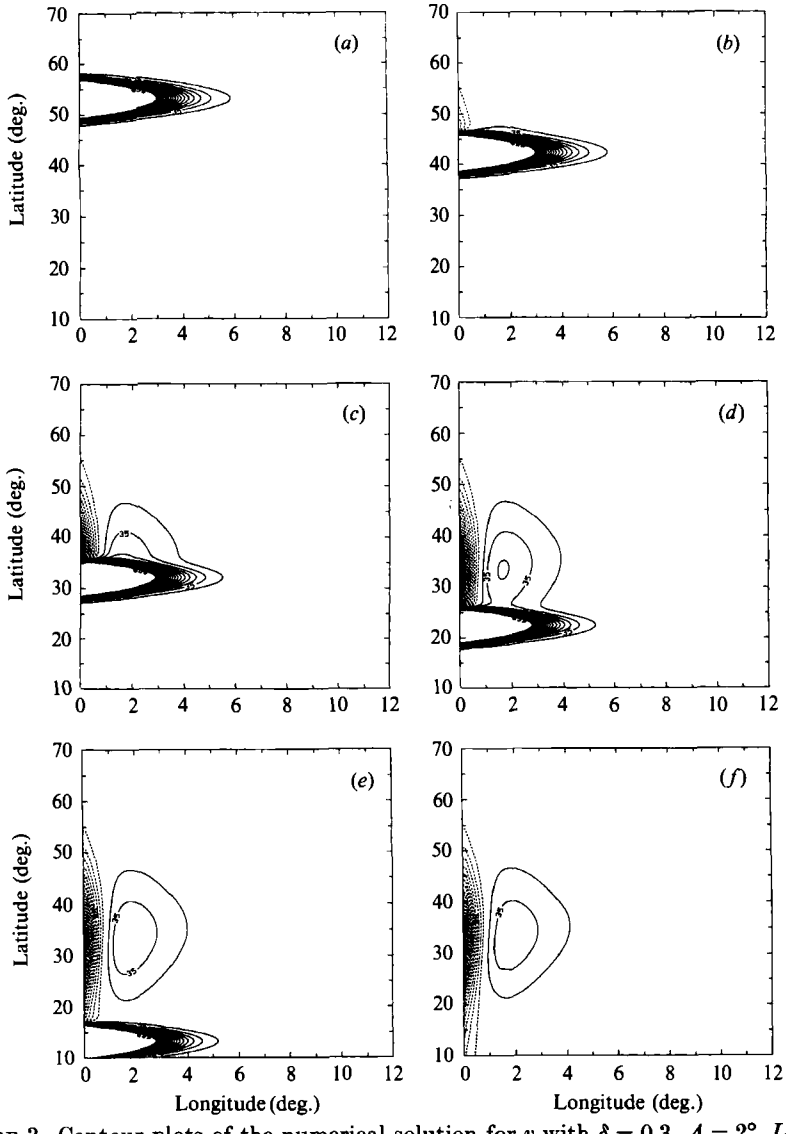

FIGURE 3. Contour plots of the numerical solution for v with $\delta = 0.3$, $A = 2°$, $L_y = 10°$ and $\Delta = 500$ at six different times. (*a*) $t = 2$; (*b*) $t = 4$; (*c*) $t = 6$; (*d*) $t = 8$; (*e*) $t = 10$; (*f*) $t = 12$ days.

the WKB condition, so that one anticipates that the evolution of the wave should follow the theoretical predictions obtained in the previous sections. In particular, since we have chosen a very small amplitude, the numerical solutions should remain in the linear regime and the evolution the Kelvin wave should obey Green's law.

In figures 3 and 4 contour plots of the solutions for v and h are shown at six different times. Consistent with the theoretical prediction we see that a residual circulation gradually develops in the wake of the wave pulse. At $t = 12$ days the Kelvin wave pulse has completely travelled over the topography; the recirculation pattern left behind looks very similar to asymptotic solutions shown in figure 2. To

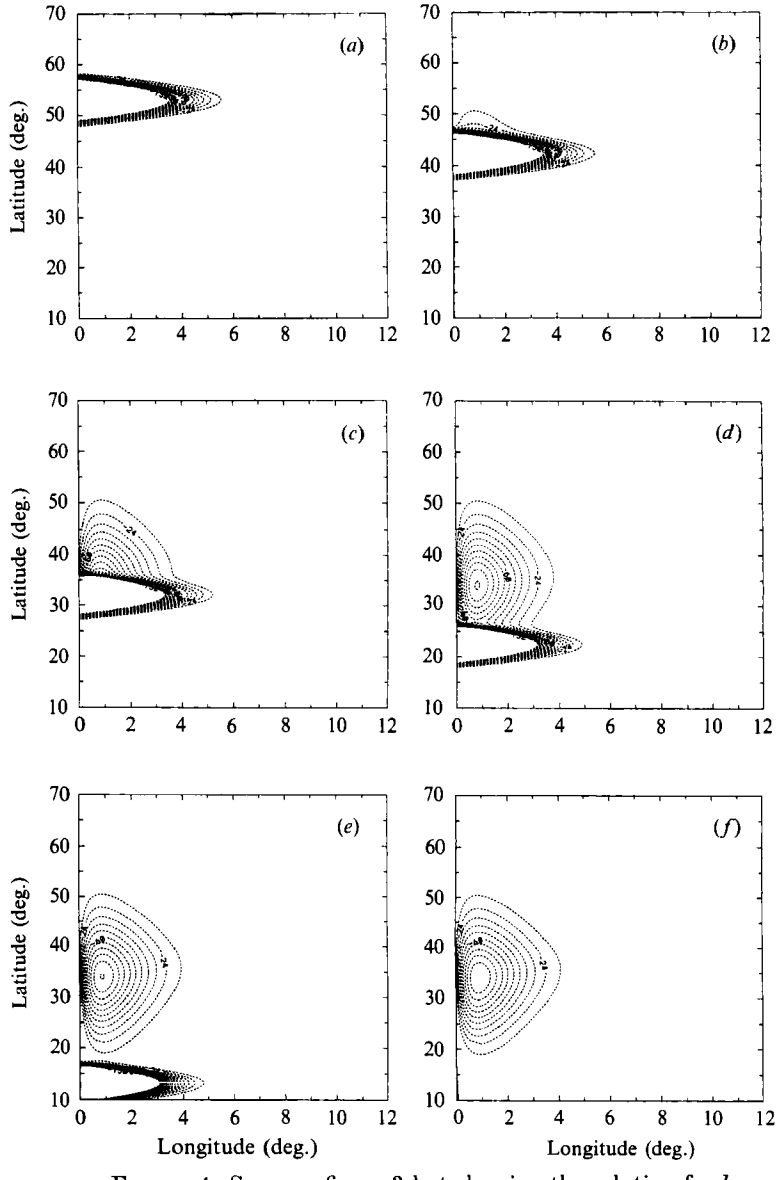

FIGURE 4. Same as figure 3 but showing the solution for h.

have a quantitative comparison between the numerical and the asymptotic solutions, we computed the relative error of the residual mass

$$E_m = \frac{\left|\iint h_a \, dx \, dy - \iint h_n \, dx \, dy\right|}{\left|\iint h_a \, dx \, dy\right|} = 5.474\,\%,$$

where h_n denotes the residual height field obtained numerically at $t = 12$ days and h_a

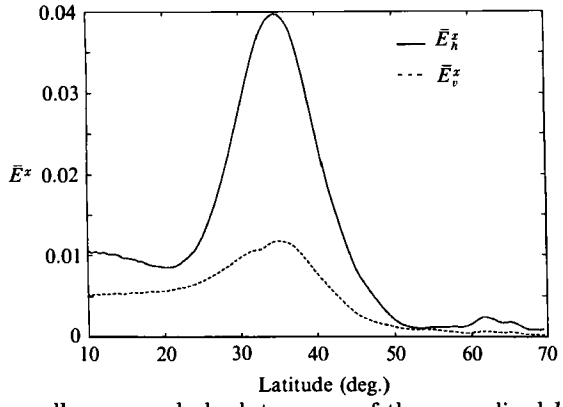

FIGURE 5. The zonally averaged absolute errors of the normalized h and v, $\bar{E}_h^x$ and $\bar{E}_v^x$, as a function of latitude. The maximum errors occur along the centre of the topography at $y = 35°$.

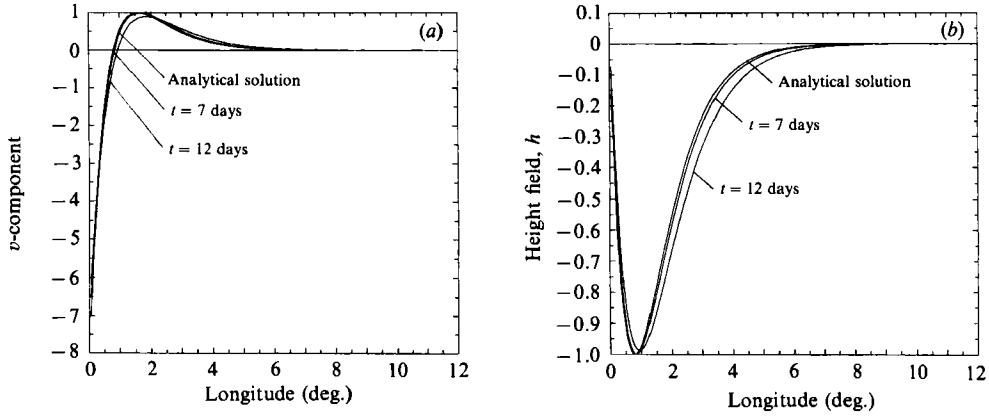

FIGURE 6. Transverse profiles of (*a*) v and (*b*) h plotted along the centre of the topography.

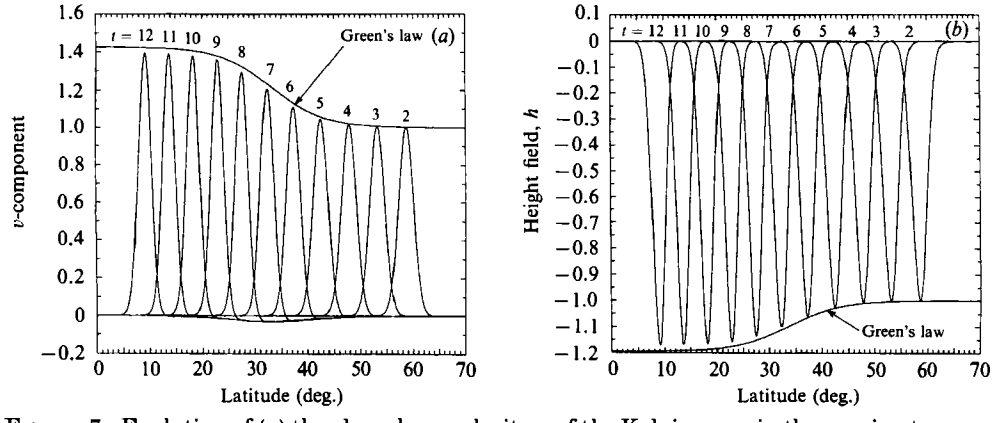

FIGURE 7. Evolution of (*a*) the alongshore velocity v of the Kelvin wave in the varying topography along the boundary and (*b*) the height field h. The numbers in this and subsequent similar figures indicates the time (days) at which the numerical solution is plotted.

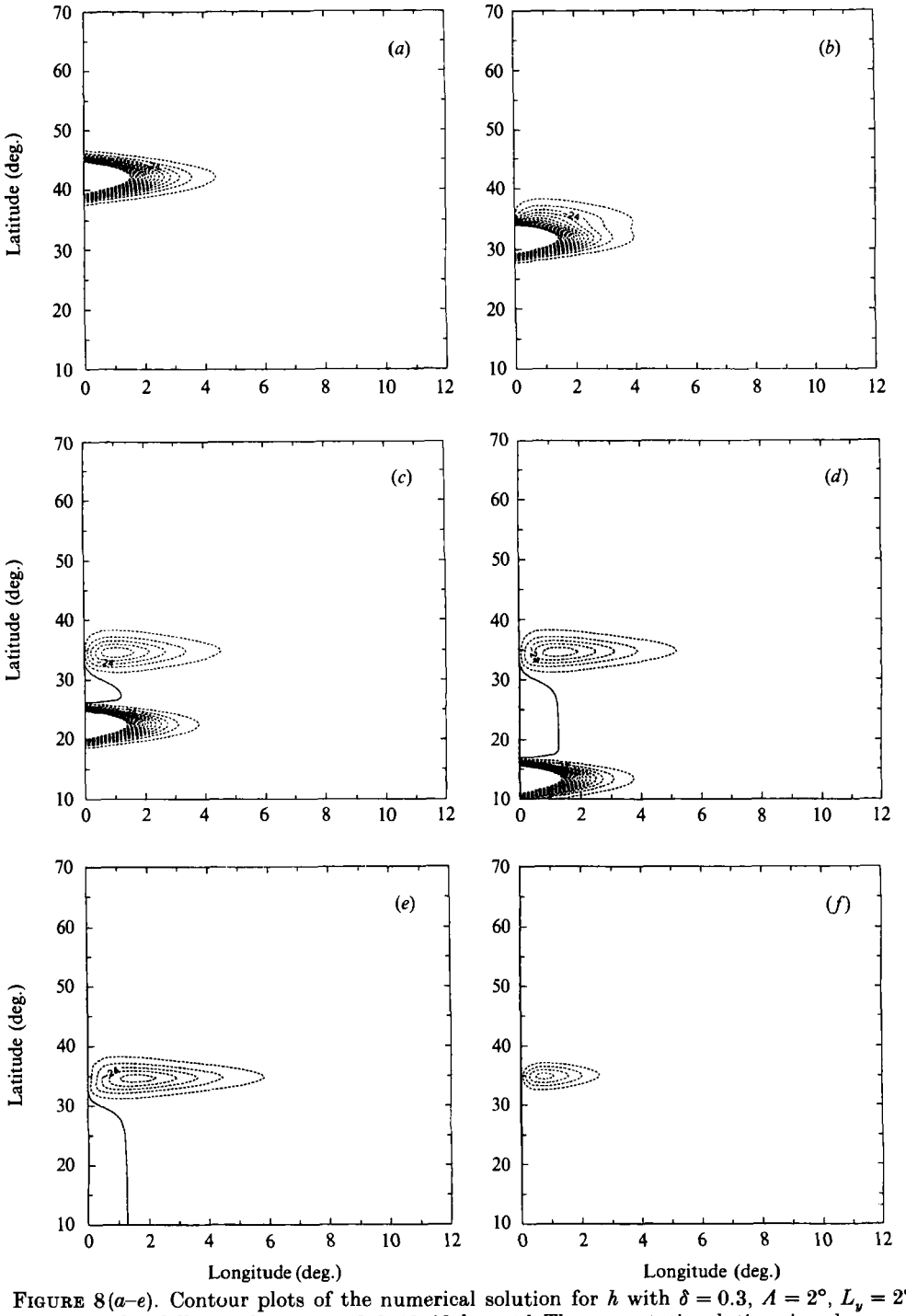

FIGURE 8(*a–e*). Contour plots of the numerical solution for h with $\delta = 0.3$, $\Lambda = 2°$, $L_y = 2°$ and $\Delta = 500$ at five different times $t = 4, 6, 8, 10, 12$ days. (*f*) The asymptotic solution given by equations (37) in the text.

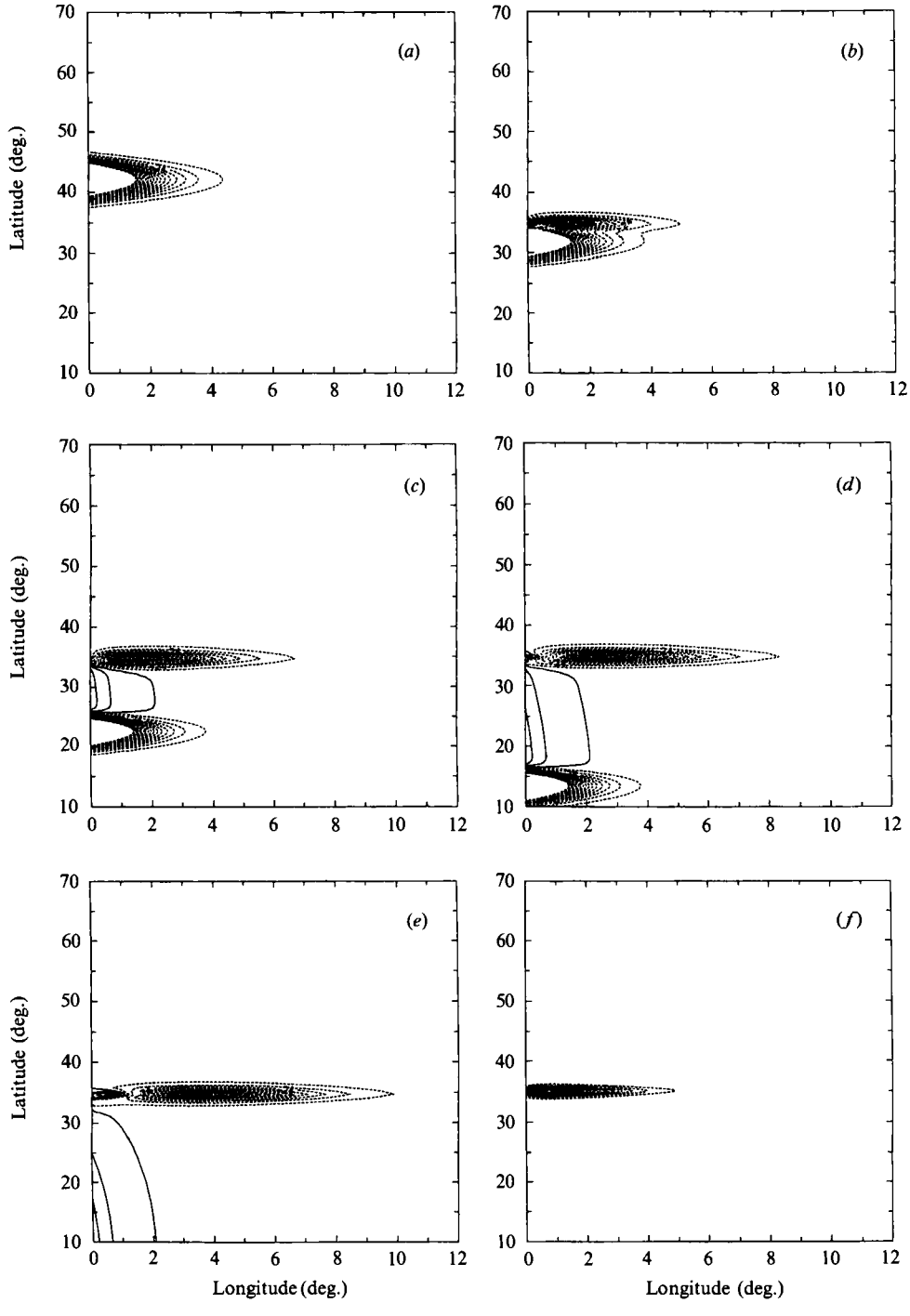

FIGURE 9. Same as figure 8 but for narrower topography with $L_y = 0.5°$.

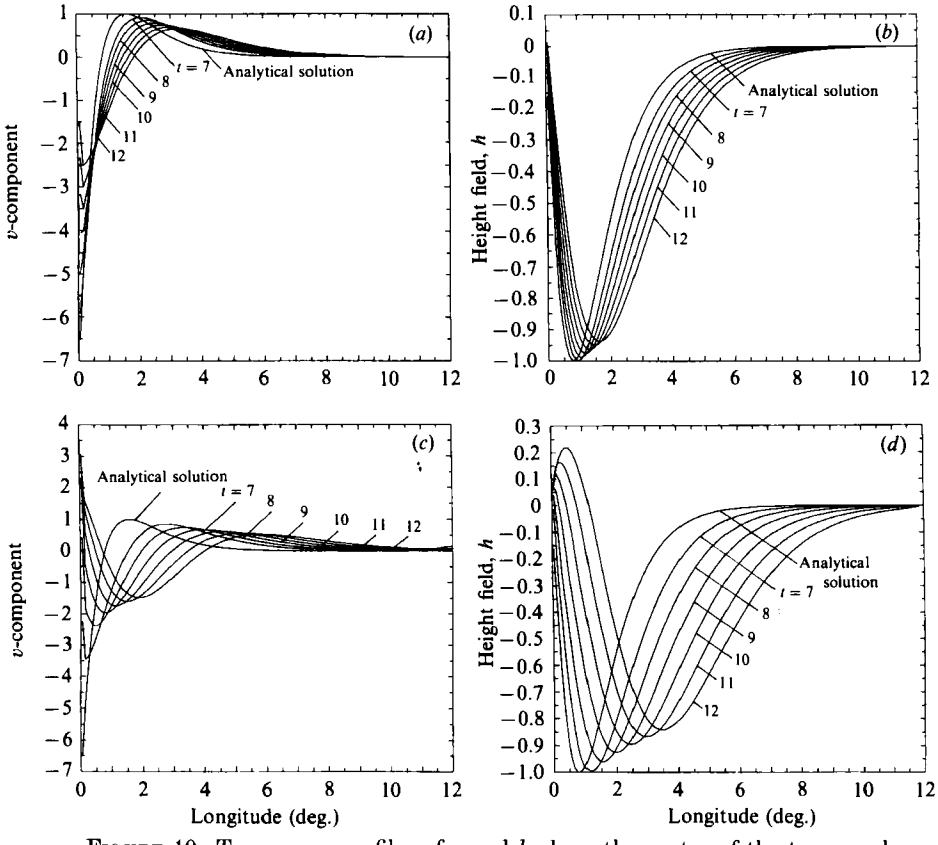

FIGURE 10. Transverse profiles of v and h along the centre of the topography: (*a*) v with $L_y = 2°$; (*b*) h with $L_y = 2°$; (*c*) v with $L_y = 0.5°$; (*d*) h with $L_y = 0.5°$.

is the asymptotic solution as $t \to \infty$. The domain-averaged absolute errors of normalized height field h and alongshore velocity component v are

$$E_h = \frac{\left|\iint (h_a - h_n)\,dx\,dy\right|}{\iint dx\,dy} = 0.0121, \quad E_v = \frac{\left|\iint (v_a - v_n)\,dx\,dy\right|}{\iint dx\,dy} = 0.0047,$$

respectively. These figures indicate that the numerical solutions overall agree well with the asymptotic solutions.

The maximum errors between the numerical and asymptotic solutions occurred along the centre of the topography at $y = 35°$, as indicated in figure 5, which shows the zonally averaged absolute errors of h and v as a function of latitude. These large errors are caused by a slow propagation of the numerical solution of the residual circulation in the offshore direction. Figure 6 shows the transverse structure of the residual circulation along the centre of the topography ($y = 35°$). The analytical solutions agree very well with the numerical solutions at $t = 7$ days (when the wave pulse has just passed the centre of the topography ($y = 35°$)). At $t = 12$ days, the numerical solutions exhibit a slight shift of v and h towards the east. This offshore propagation may be attributed to the topographic Rossby waves whose propagation speed depends on the slope of the topography. In this experiment, we have chosen

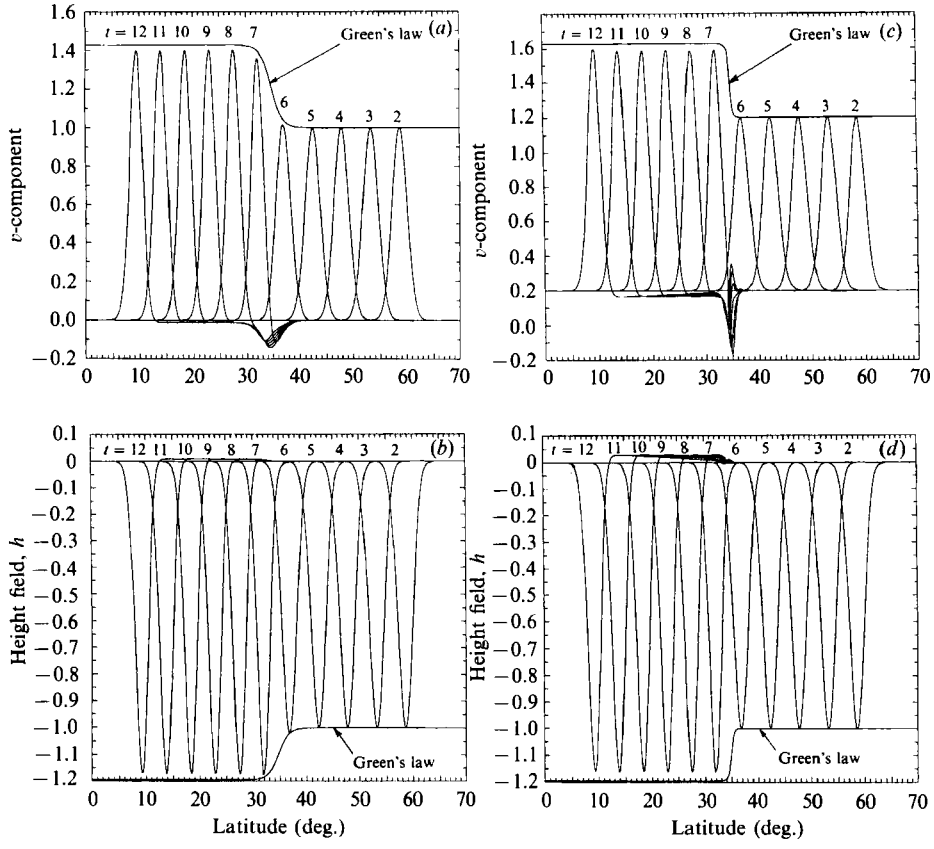

FIGURE 11. Same as figure 7 but for narrow-topography experiments: (*a*) v with $L_y = 2°$; (*b*) h with $L_y = 2°$; (*c*) v with $L_y = 0.5°$; (*d*) h with $L_y = 0.5°$.

a very small slope in order to compare with our analytic solutions, so that the transverse propagation is negligible small. The estimated offshore propagation speed of the centroid of the height field h along $y = 35°$ is about 4.713×10^{-2} m/s which is two orders of magnitude smaller than the phase speed of the Kelvin wave (7 m/s in this case). This feature, however, will be changed when the alongshore lengthscale of the topography becomes comparable to or smaller than the scale of the wave, as we will see in the following experiments.

Figure 7 shows the wave amplitude evolution of v and h along $x = 0$. The model outputs along the boundary at times $t = 2, 3, \ldots, 12$ days are displayed in figures 7 (*a*) and 7 (*b*) respectively. Superimposed are the results obtained from Green's law which predicts that v and h vary as the layer depth $H(y)$ to the power of -1 and $-\frac{1}{2}$, respectively. As one can see, both of the figures show an excellent agreement between the numerical and asymptotic calculations.

In the next two experiments, we reduced the lengthscale of the topography to $L_y = 2°$ and $L_y = 0.5°$. Figures 8 and 9 are 'snapshots' of h taken at $t = 4, 6, 8, 10$ and 12 days for the two experiments. In contrast to the analytical solutions shown in figures 8 (*f*) and 9 (*f*), residual circulation obtained from the numerical model rapidly expands eastward after its generation by the Kelvin wave pulse. This feature is further illustrated in figure 10 which shows the time evolution of v and h along $y = 35°$. Evidently, the eastward propagation of the residual circulation is controlled by

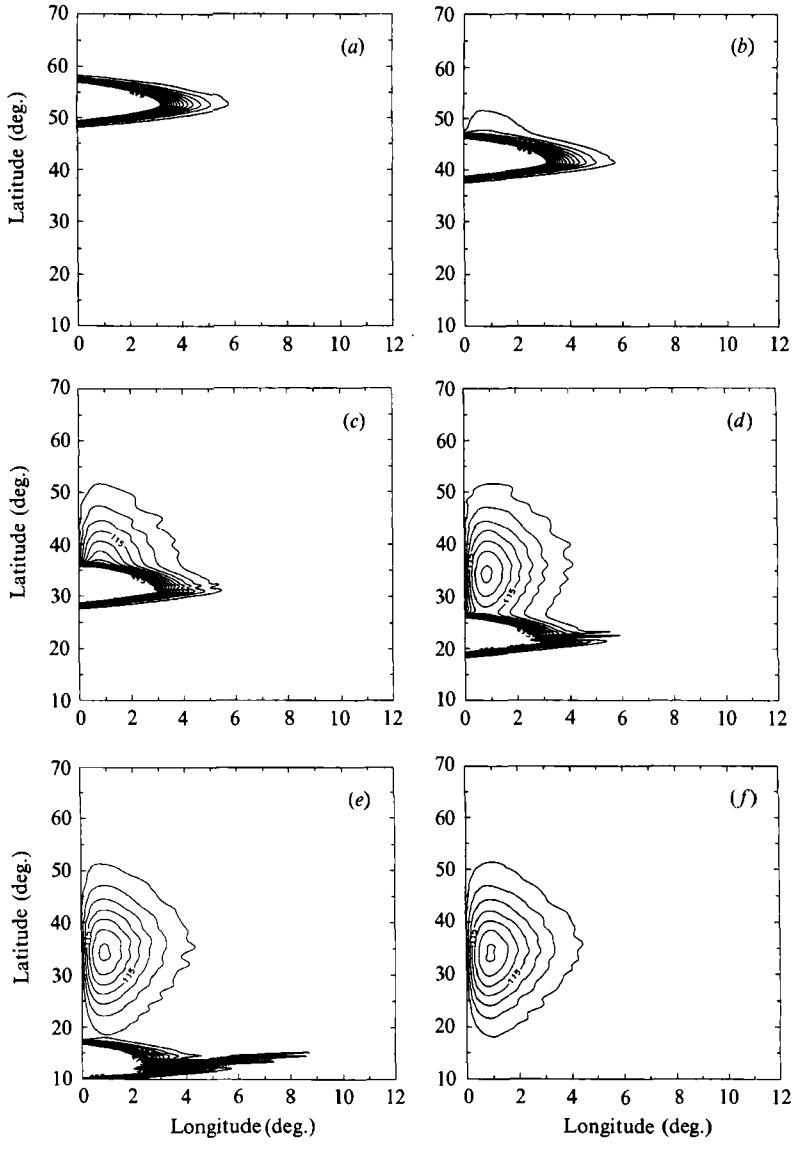

FIGURE 12. Same as figure 4 except that in this case the amplitude of the wave is increased by a factor of 20 with $A = 25$.

the slope of the topography. The bigger the slope is, the faster is the transverse propagation. This result suggests that the topographic Rossby waves are important in the adjustment of the residual mass when the lengthscale of the topography becomes comparable to or smaller than the scale of the wave pulse. The WKB solutions obtained in §3 break down because the lengthscale of the topography is comparable to the scale of the wave. In this case topographic waves may have effects on both the primary Kelvin wave and residual mass adjustment as explained in §3. However, it is interesting to note that even in this case the amplitude evolution of the Kelvin wave agrees well with the Green law, as shown in figure 11. It is also interesting to note from figure 11 that a secondary structure – a shelf which extends between the primary wave and the residual mass over the topography – is created.

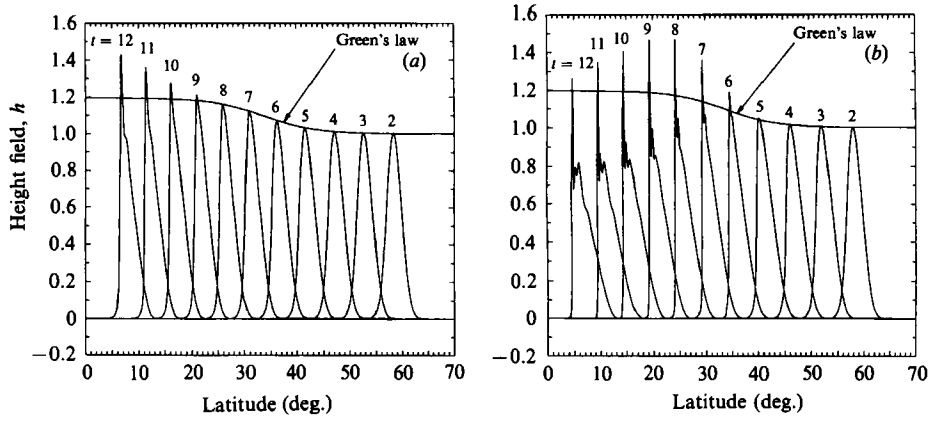

FIGURE 13. Evolution of the Kelvin wave amplitude in h along the boundary $x = 0$ in the varying topography for (*a*) $\Delta = 25$ and (*b*) $\Delta = 10$.

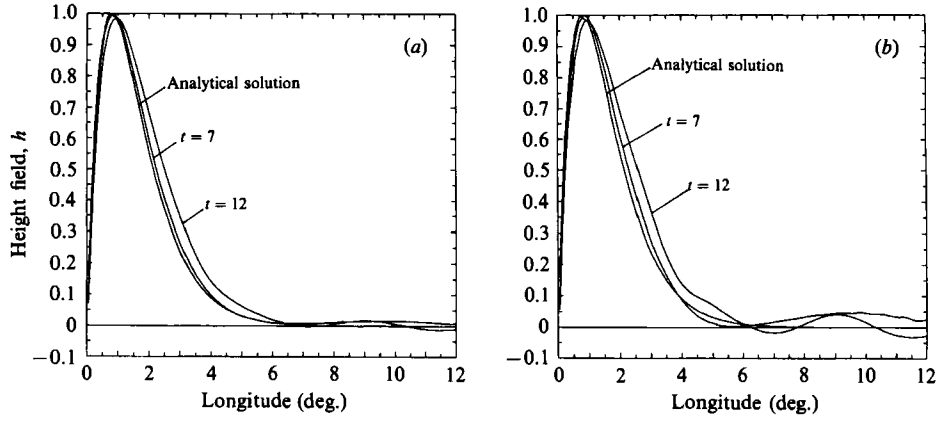

FIGURE 14. Transverse profiles of h along the centre of the topography for (*a*) $\Delta = 25$ and (*b*) $\Delta = 10$.

This shelf seems to be trapped near the boundary, as shown in figures 8 and 9. No explanation about this secondary structure is given here.

Finally, we examine the effects due to finite wave amplitude. We present the results from two numerical experiments with $\Delta = 25$ and $\Delta = 10$. Since the offshore topographic variation is not included, the Kelvin wave remains non-dispersive. This means that the almost inevitable consequence of nonlinearity is shock waves. In figure 12 we present contour plots of h at six different times for $\Delta = 25$. In comparison with the small-amplitude experiment shown in figure 4, the development of the residual circulation behind the leading-order Kelvin wave appears to be similar except for the superimposed small-scale wave disturbances. The main difference is associated with the primary Kelvin wave pulse. At about $t = 6$ days, one can see that the wave front is considerably steepened and small-scale wave disturbances start to develop at the edge of the wave front. Thus, energy is no longer concentrated within a radius of deformation of the coast: instead there appears to be an energetic zone trailing from the head of the wave front, this trailing streamer consisting of very small-scale wave disturbances and becoming more extensive with time. Furthermore, a 'lie-back' angle between the streamer and the normal to the coast can be clearly

identified in figure 12. Anderson (1981) has argued that the trailing streamer is attributable to the Poincaré waves. Because these waves can only travel at a maximum speed determined by the local depth of the fluid ($C = (g'H)^{\frac{1}{2}}$), they cannot keep up with the nonlinear Kelvin wave front and thus fall behind. Recently, Melville, Tomasson & Renouard (1980) have shown both analytically and numerically that a small increase in the Kelvin wave speed due to nonlinearity may lead to a direct resonance with the linear Poincaré waves. Therefore, energy will be transferred continuously from the Kelvin wave to the Poincaré waves, resulting in the curvature of the wave front. The amplitude evolution of h along the boundary shown in figure 13 for both $\Delta = 25$ and $\Delta = 10$ indicates that Green's law, as expected, fails to describe the wave amplitude evolution after breaking occurs. This means that the wave energy is no longer conserved. Figure 13 further indicates that the amplitude of the wave front overshoots the value predicted by the linear theory. However, this result cannot be taken seriously because the numerical scheme adopted here cannot handle the shock waves accurately. Nevertheless, the feature associated with the generation of residual circulation seems to be robust even for large-amplitude Kelvin waves. The transverse structure of the residual circulation shown in figure 14 again indicates a good agreement between the theoretical and numerical solution except in the region far off the coast where weak wave-like disturbances can be seen in the numerical solutions.

5. Discussion

One of the most powerful dynamic constraints on the fluid motion in an inviscid rotating fluid is that the potential vorticity Q must be conserved following the fluid particles, namely

$$\frac{\partial Q}{\partial t} + u\frac{\partial Q}{\partial x} + v\frac{\partial Q}{\partial y} = 0, \tag{41}$$

where

$$Q = \left(f + \frac{\partial v}{\partial x} - \frac{\partial u}{\partial y}\right) \Big/ (\bar{h} + h).$$

This dynamic constraint may be used to understand the physical mechanism associated with the generation of residual mass as a Kelvin wave pulse passes through a slowly varying topography.

Imagine that a small-amplitude ($O(\epsilon)$) Kelvin wave has just passed by a location y, the pressure pulse associated with the wave pushes the fluid particles through a small distance of $O(\epsilon)$. This $O(\epsilon)$ displacement of fluid particles will then cause an $O(\epsilon^2)$ change in the fluid depth H, because the slowly varying topography allows only an $O(\epsilon)$ change in depth over a distance of $O(1)$. For a small-amplitude disturbance ($O(\epsilon)$), the potential vorticity Q can be expanded in a power series in ϵ:

$$Q = \frac{f}{H} + \frac{\epsilon}{H}Q_0' + \frac{\epsilon^2}{H}\left[Q_1' - \frac{h_0}{H}Q_0'\right] + O(\epsilon^3), \tag{42}$$

where

$$Q_i' = \left(\frac{\partial v_i}{\partial x} - \frac{\partial u_i}{\partial y}\right) + \frac{f h_i}{H} \quad (i = 0, 1),$$

is the perturbed potential vorticity at $O(\epsilon)$ and $O(\epsilon^2)$, and u_i, v_i, h_i ($i = 0, 1$) are our perturbation solutions. Since the total potential vorticity is conserved following the fluid particles, an $O(\epsilon^2)$ change in ambient potential vorticity induced by an $O(\epsilon)$

displacement of fluid particles must be compensated by the same amount of change in the perturbed potential vorticity Q'. Substituting the Kelvin wave solution (7)–(9) into the perturbed potential vorticity Q', it is easy to verify that the perturbed potential vorticity associated with the Kelvin wave is identically equal to zero, namely, $Q'_0 = 0$. This result indicates that Kelvin waves carry no perturbed potential vorticity. Since Q'_0 is equal to zero, it follows immediately from (42) that the potential vorticity anomalies can only be generated at $O(\epsilon^2)$. Once these potential vorticity anomalies are created, they cannot be carried away by either Kelvin waves or Poincaré waves. Instead they will remain behind to establish a geostrophic equilibrium by radiating Poincaré waves and a Kelvin wave. Consequently, the residual mass is created over the topography. This process is very similar to the classical geostrophic adjustment considered by Rossby (1937, 1938), Blumen (1972) and Gill (1976, 1982).

Of course, the adjustment process will be altered if vorticity waves (namely Rossby waves) must be taken into account, because these waves can carry potential vorticity anomalies as they propagate in space. This is the case when the lengthscale of the topography is comparable to or smaller than the scale of the Kelvin wave, as demonstrated by the numerical experiments in §4. The westward-propagating equatorial Rossby waves also play an important role in the adjustment of potential vorticity anomalies generated by an equatorial Kelvin wave propagating in a slowly varying thermocline (Long & Chang 1990). The residual mass in this case was found to be reflected by westward-propagating Rossby waves. This mechanism of generation of residual circulation will also operate in the situation when a Kelvin wave propagates along a lateral ocean boundary on the spherical Earth, except that in this case the change in ambient potential vorticity is produced by the change in Coriolis parameter rather than in the depth of the fluid. However, the adjustment process may be complicated by the equatorially trapped waves as the Kelvin wave approaches the equator. This problem is now under investigation.

I wish to express my gratitude to Professor R. Grimshaw for making critical comments that improved the paper considerably. He also pointed out a different approach to solve the problem (see the footnote in §2). I am grateful to Dr B. Long for helpful discussion during the course of this work. I also thank the anonymous referee for valuable comments about this paper. The work was supported by NOAA/JISAO grant NA90RAH000073. This is a contribution to JISAO. Contribution number 113 of JISAO/University of Washington.

REFERENCES

Anderson, D. L. T. 1981 Cross-equatorial waves, with applications to the low-level east-African jet. *Astrophys. Fluid Dyn.* **16**, 267–284.

Arakawa, A. & Lamb, V. 1977 Computational design of the basic dynamical process of the UCLA general circulation model. In *Methods in Computational Physics*, vol. 17, pp. 173–265. Academic.

Arakawa, A. & Lamb, V. 1981 A potential enstrophy and energy conserving scheme for the shallow water equations. *Mon. Wea. Rev.* **109**, 18–36.

Blumen, W. 1972 Geostrophic adjustment. *Rev. Geophys. Space Phys.* **10**, 485–528.

Gill, A. E. 1976 Adjustment under gravity in a rotating channel. *J. Fluid Mech.* **77**, 603–621.

Gill, A. E. 1982 *Atmosphere–Ocean Dynamics.* Academic, 662 pp.

Grimshaw, R. 1977 Nonlinear aspects of long shelf waves. *Geophys. Astrophys. Fluid Dyn.* **8**, 3–16.

GRIMSHAW, R. 1983 Solitary waves in slowly varying environments: long nonlinear waves. In *Nonlinear Waves* (ed. L. Debnath). Cambridge University Press, 360 pp.

JOHNSON, R. 1973 On the asymptotic solution of the Korteweg–de Vries equation with slowly varying coefficient. *J. Fluid Mech.* **60**, 313–324.

KAKUTANI, T. 1971 Effects of an uneven bottom on gravity waves. *J. Phys. Soc. Japan* **30**, 272–276.

KILLWORTH. P. D. 1989*a* How much of a baroclinic coastal Kelvin wave gets over a ridge? *J. Phys. Oceanogr.* **19**, 321–341.

KILLWORTH. P. D. 1989*b* Transmission of a two-layer coastal Kelvin wave over a ridge. *J. Phys. Oceanogr.* **19**, 1131–1148.

KNICKERBOCKER, C. J. & NEWELL, A. C. 1980 Shelves and the Korteweg–de Vries equation. *J. Fluid Mech.* **98**, 803–818.

KNICKERBOCKER, C. J. & NEWELL, A. C. 1985 Reflections from a solitary wave in a channel of varying depth. *J. Fluid Mech.* **153**, 1–16.

LONG, B. & CHANG, P. 1990 Propagation of an equatorial Kelvin wave in a varying thermocline. *J. Phys. Oceanogr.* **20**, 1826–1841.

MELVILLE, W. K., TOMASSON, G. G. & RENOUARD, D. P. 1989 On the stability of Kelvin waves. *J. Fluid Mech.* **206**, 1–23.

MILES, J. W. 1972 Kelvin waves on oceanic boundaries. *J. Fluid Mech.* **55**, 113–127.

MILES, J. W. 1973 Kelvin-wave diffraction by changes in depth. *J. Fluid Mech.* **57**, 401–413.

MILES, J. W. 1979 On the Korteweg–de Vries equation for a gradually varying channel. *J. Fluid Mech.* **91**, 181–190.

NEWELL, A. C. 1985 *Solitons in Mathematics and Physics.* Philadelphia, Pa: SIAM, pp. 244.

ROSSBY, C. G. 1937 On the mutual adjustment of pressure and velocity distributions in certain simple current systems. I. *J. Mar. Res.* **1**, 15–28.

ROSSBY, C. G. 1938 On the mutual adjustment of pressure and velocity distributions in certain simple current systems. II. *J. Mar. Res.* **2**, 239–263.

SMITH, R. 1972 Nonlinear Kelvin and continental-shelf waves. *J. Fluid Mech.* **52**, 379–391.